15th IFK
Proc. of the 15th International Fluid Power Conference <Symposium/Conference>
<DOI>

# From Turbulence to Tranquillity: A Multidisciplinary Blueprint for Optimising Liquid Cooling in Precision Machinery

**Enrico Pasquini[1], Jonas Wack[1], Afshin Sattarifar[1] & Peter Gehr[2]**

[1]*AVL Deutschland GmbH, Junkers-Ring 6, 85098 Großmehring, enrico.pasquini@avl.com*

[2]*AVL Software and Functions GmbH, Im Gewerbepark B29, 93059 Regensburg*

## Abstract

High-power precision optical systems are essential for cutting-edge technology – from laser additive manufacturing and gravitational-wave interferometry to directed-energy drone defence. The encountered intense thermal loads typically require liquid cooling, even though pressure ripples and flow-induced vibrations in the coolant can undermine mechanical precision and degrade optical accuracy.

This paper introduces a multidisciplinary engineering methodology for systematically analysing and mitigating vibration issues in liquid cooling systems for highly mechanically sensitive applications. The approach integrates 1D acoustic simulation, 3D vibro-acoustic analysis, 3D computational fluid dynamics (CFD), 1D/3D thermal simulation, mechanical design, materials science, and experimental validation into a unified workflow. Its performance is demonstrated on a representative cooling circuit which, in its original state, generates unacceptably high oscillating flow forces that impair the optical performance of the overall system.

The first step in the methodology is the development of a system-level, frequency-domain 1D model to determine the baseline oscillating pressure, flow rate and force distribution throughout the cooling circuit and identify the driving mechanism of the disturbances. To cover complex components (e.g., hoses or pumps), surrogate models derived from 3D simulation or from direct experimental measurements are integrated into the 1D framework. Based on the initial results for the forces and the associated system sensitivities, mitigation measures are derived which enable a reduction of the disturbing forces by more than 90 %.

By systematically integrating multiple engineering disciplines into a unified framework, this approach represents a significant advancement over traditional, isolated analysis techniques. The ability to iteratively refine models across multiple domains ensures a robust and optimised solution for mitigating flow-related disturbances. The methodology is particularly valuable for applications requiring ultra-high precision, where even minor perturbations can severely impact system performance.

**Keywords:** Duct acoustics, precision engineering, condition number, multidomain optimisation, surrogate modelling.

# 1. INTRODUCTION

High-precision, high-power optical machinery is indispensable in the modern world. It enables ultra-accurate medical diagnostics, such as optical coherence tomography for retinal imaging, and is vital to cutting-edge, optics-based manufacturing methods (laser-based manufacturing, additive manufacturing, optical lithography). It underpins major scientific breakthroughs, such as the use of laser interferometers to detect gravitational waves, and plays a critical role in defence as well, for instance by countering drone attacks with directed energy weapons. The high thermal loads commonly encountered in such machinery typically require liquid cooling to prevent degradation in optical performance and structural failure.

However, in high-precision applications, liquid cooling is not free of cost: The presence of a coolant enables *hydraulic communication* even between components of the cooling circuit that are far apart from each other. As a result, mechanical or flow disturbances – for example, originating at the pump – can propagate to sensitive components such as a directly cooled laser beam source and adversely affect their optical performance. The issue is illustrated on the example of a cooling circuit for a high-precision optical manufacturing system.

## 1.1. Cooling System Under Consideration

In its baseline configuration, the cooling circuit comprises an external gear pump (displacement volume per rotation of 2.85 cm³ and $z$ = 9 teeth per gear), two microchannel heat exchangers (see Figure 6 for dimensions), a return tank, interconnected piping and flexible PVC hoses. A CAD model of the duct system is shown in Figure 1:

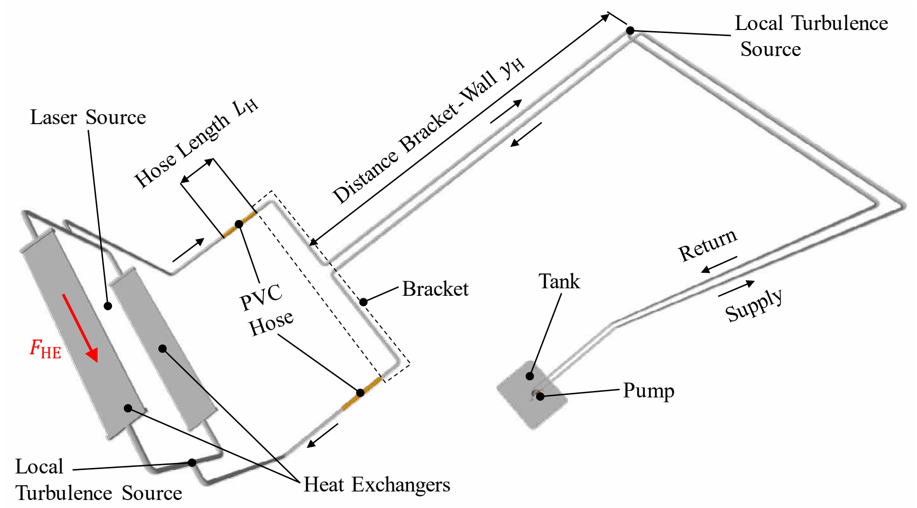


Figure 1: Cooling system under consideration.

The highly mechanically sensitive laser source is directly mounted between both heat exchangers. To be able to adjust the laser beam’s orientation during operation, the beam source – and thus its piping – must be suspended in a movable manner. This is achieved by two hoses within the routing.

### 1.2. Precision Losses and their Mitigation

During initial commissioning of a prototype of the system, it was observed that the operation of the cooling system was associated with unacceptably high optical precision losses due to unbalanced forces acting on the laser beam source, see Figure 1.

In order to effectively suppress the disturbing oscillatory forces, suitable – preferably passive – mitigation measures are to be taken. Because the mechanical design of the rest of the machine is already comparatively mature, major structural changes on the laser source and its support and actuator system are not possible anymore. Therefore, a direct reduction of the hydraulic excitation is necessary. Due to space constraints, the use of bulky resonators and silencers is not possible, leaving the adjustment of the position and length of the already existing hoses as the only viable option.

Before any mitigation strategy can be designed, the operating modes of the system need to be identified. The duct circuit acts as an oscillatory system which consists of fluid (coolant) and solid (duct walls, valve housing) elements. Both the fluid and the solid elements possess compliance and inertia. Thus, the unsteady forces and moments exerted by the duct system on the laser source result from the response of this oscillatory system to external as well as internal stimuli. In many applications, the inertia and most of the compliances of the solid parts can be neglected (weak fluid-structure interaction), such that the oscillatory forces acting on the duct structure are primarily a result of the pressure fluctuations at directional changes (e.g. bends) or area changes (e.g. conical sections) of the duct system.

In this case, the estimation of the oscillatory forces and moments reduces to determining the unsteady pressure and flow field in the duct system – a field commonly referred to as *duct acoustics*.

## 2. FUNDAMENTALS OF DUCT ACOUSTICS

In order to investigate the flow and pressure oscillations in a duct system by numerical analysis, a suitable model depth must be selected for each component. Depending on the properties of the individual component, either a 0D, 1D or 3D model must be chosen.

### 2.1. 0D vs. 1D vs. 3D Models

0D models are most suitable if the internal degrees of freedom of a component are not of relevance to its transmission behaviour. This is the case if the travel time $L/c$ of a pressure wave of speed $c$ through a component of characteristic length $L$ is substantially smaller than the period $1/f$ of the frequency of interest, i.e. $fLc^{-1} \ll 1$. A typical example would be the model of a small return tank, where the pressure can be assumed to be uniform throughout the component and internal wave propagation is not of concern. Also, for a sufficiently short pipe section, compressibility effects can be ignored, such that the flow rate is constant along the section length. If the product $fLc^{-1}$ is not small with respect to unity, wave phenomena within the component need to be considered. If the wave propagation primarily occurs along a single dimension (e.g. along the longitudinal axis of a slender pipe section), 1D models suffice. If even this simplification does not apply and substantial changes of state variables might occur along more than one spatial dimension, one is required to resort to 2D or even 3D models. For most components encountered in duct acoustics, 1D models suffice.

## 2.2. Frequency vs. Time Domain Analysis

Irrespective of the chosen model depth, a choice must be made whether the system analysis is to be carried out in the time or frequency domain. Table 1 provides an overview over various aspects that drive the decision between time and frequency domain analysis.

Table 1: Comparative capability analysis of time vs. frequency domain analysis.

| Aspects | Time Domain | Frequency Domain |
|---|---|---|
| Analysis of Transients<br>(Valve closure & pump ramp-up) | ✓ | ✗ (Only linearised) |
| Consideration of system nonlinearities<br>(Cavitation, large amplitudes) | ✓ | ✗ (Only linearised) |
| Determination of Steady-state modes,<br>resonances & transfer functions | ✓ (Slow) | ✓ |
| Acoustic optimisation<br>(Silencer design, shifting of resonances) | ✓ (Very slow) | ✓ |
| Efficient for large range of frequencies | ✗ (Large amounts of data, extremely slow) | ✓ |

For the cooling circuit under consideration, only steady-state oscillations are of interest and the amplitudes are small, such that frequency-domain simulation can demonstrate its advantages. If the analysis is limited to the frequency domain, the computationally efficient *transfer matrix method* can be employed.

## 2.3. Transfer Matrix Method

In the case of a 1D hydraulic system model, both pressure $p$ and flow rate $Q$ are required to uniquely describe the flow state at a given cross-section. Thus, to characterise the relation between the states at the inlet and outlet of any 1D component in the frequency domain, the concept of a transfer function has to be generalised to a transfer matrix $\boldsymbol{T}$. This generally frequency-dependent and complex-valued function relates the phasor vectors at the inlet with those at the outlet:

$$\begin{pmatrix} p_{\mathrm{In}}^* \\ Q_{\mathrm{In}}^* \end{pmatrix} = \boldsymbol{T} \begin{pmatrix} p_{\mathrm{Out}}^* \\ Q_{\mathrm{Out}}^* \end{pmatrix} = \begin{bmatrix} T_{11} & T_{12} \\ T_{21} & T_{22} \end{bmatrix} \begin{pmatrix} p_{\mathrm{Out}}^* \\ Q_{\mathrm{Out}}^* \end{pmatrix} \tag{2.1}$$

For example, the transfer matrix $\boldsymbol{T}_{\mathrm{Pipe}}$ of a straight circular pipe of length $L$ and cross-sectional area $A$, filled with an inviscid fluid of sonic speed $c$, is given by:

$$\boldsymbol{T}_{\text{Pipe}} = \begin{bmatrix} \cosh\left(\frac{\mathrm{i}\omega L}{c}\right) & \frac{\rho c}{A}\sinh\left(\frac{\mathrm{i}\omega L}{c}\right) \\ \frac{A}{\rho c}\sinh\left(\frac{\mathrm{i}\omega L}{c}\right) & \cosh\left(\frac{\mathrm{i}\omega L}{c}\right) \end{bmatrix} = \begin{bmatrix} \cos\left(\frac{\omega L}{c}\right) & \frac{\mathrm{i}\rho c}{A}\sin\left(\frac{\omega L}{c}\right) \\ \frac{\mathrm{i}A}{\rho c}\sin\left(\frac{\omega L}{c}\right) & \cos\left(\frac{\omega L}{c}\right) \end{bmatrix} \tag{2.2}$$

The transfer matrix of a series connection of two components A and B is readily obtained by matrix multiplication of the respective matrices $T_{\mathrm{A}}$ and $T_{\mathrm{B}}$. Further details regarding the interconnection and usage of transfer matrices can be found in the literature [1][2]. By combining multiple matrix elements, a system model as described in section 3 can be set-up. For components whose transfer matrix cannot be determined by analytical estimates, experimental methods have to be employed.

## 2.4. TMM Test Bench

For the experimental determination of the transfer matrix of a specific component, a so-called transfer matrix method (TMM) test bench as shown in Figure 2 is used [3].

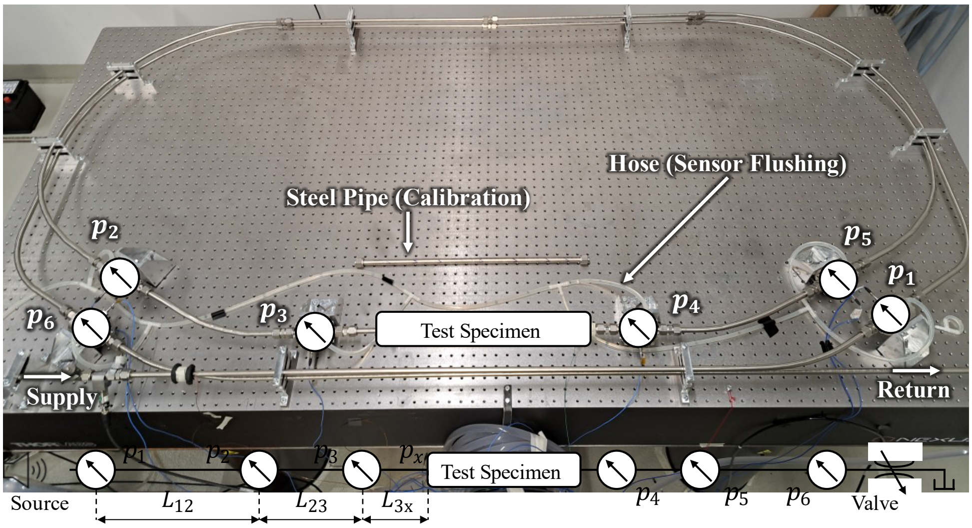


Figure 2: AVL Transfer Matrix Method Test Bench.

The test bench consists of up to six unsteady ("dynamic") pressure transducers, a load valve and a suitable acoustic source. The source as well as the valve must be located either before the first sensor or after the last sensor. The acoustic source excites the system and creates a wave pattern that is characteristic for the system under investigation.

### 2.4.1. Transfer Matrix Determination

To determine the transfer matrix $\boldsymbol{T}$ of a component experimentally, the phasors of pressure and flow rate at both the component inlet and outlet must be known to solve equation 2.1 for the matrix elements $T_{\mathrm{ij}}$. Since there are only two equations for four unknowns $T_{\mathrm{ij}}$, two distinctly different measurements have to be carried out to create four independent equations. This is typically achieved by adjusting the load valve to force a different wave pattern. For the specific case of a symmetric transfer behaviour of the investigated component, only one measurement is required.

Compared to measuring unsteady pressures, non-invasive measurement of unsteady flow rates is technically challenging. To overcome this, the TMM replaces the direct measurement of a single flow rate with the measurement of two unsteady pressures by utilising a rearranged form of equation 2.1:

$$p_{\mathrm{In}}^* = p_{\mathrm{Out}}^* \cdot T_{11} + Q_{\mathrm{Out}}^* \cdot T_{12} \rightarrow Q_{\mathrm{Out}}^* = \frac{p_{\mathrm{In}}^*}{T_{12}} - p_{\mathrm{Out}}^* \frac{T_{11}}{T_{12}}. \tag{2.3}$$

Thus, if two pressures and the TFM elements of the components between the pressure sensors are known, a flow rate can be determined. Because their TFM elements can be calculated with high accuracy by equation 2.2 (or more advanced models), steel pipes are used between the sensors. In the actual measurement, three instead of two sensors are used for state determination in order to expand the frequency range that can be analysed. Based on the three pressures per side and known transfer behaviour of the steel pipes between the sensors, the states at the inlet and the outlet of the test specimen can be estimated by solving the following equation system for the unknown phasors $p_x^*$ and $Q_x^*$ at a location $x$ (only shown for sensors 1, 2 and 3, see Figure 2):

$$\underbrace{\begin{pmatrix} p_1^* \\ p_2^* \\ p_3^* \end{pmatrix}}_{\vec{b}} = \begin{bmatrix} \cosh\left(\frac{\mathrm{i}\omega L_{1x}}{c}\right) & \sinh\left(\frac{\mathrm{i}\omega L_{1x}}{c}\right) \\ \cosh\left(\frac{\mathrm{i}\omega L_{2x}}{c}\right) & \sinh\left(\frac{\mathrm{i}\omega L_{2x}}{c}\right) \\ \cosh\left(\frac{\mathrm{i}\omega L_{3x}}{c}\right) & \sinh\left(\frac{\mathrm{i}\omega L_{3x}}{c}\right) \end{bmatrix} \underbrace{\begin{pmatrix} p_x^* \\ \frac{\rho c}{A} Q_x^* \end{pmatrix}}_{\vec{x}} = \boldsymbol{A} \begin{pmatrix} p_x^* \\ Z_{\mathrm{C}} Q_x^* \end{pmatrix} \tag{2.4}$$

The determination of the states – and thus the transfer matrix of the specimen – becomes challenging if the signal-to-noise ratio assumes small values. Disturbing noise levels are particularly relevant in the low-frequency range. The accuracy of experimental results in this part of the spectrum can be improved by optimising the sensor spacing.

### 2.4.2. Numerical Conditioning and Sensor Spacing

When solving a linear equation system $\vec{b} = \boldsymbol{A}\vec{x}$ like equation 2.4 for $\vec{x}$, the sensitivity to errors (i.e. noise) in $\vec{b}$ can be quantified through the so-called *condition number* $\kappa(\boldsymbol{A})$. It is defined as the ratio of the largest to the smallest singular value of $\boldsymbol{A}$. Large condition numbers imply that small errors in the measured pressures $\vec{b}$ can lead to large errors in the estimated acoustic states $\vec{x}$, whereas condition numbers close to unity indicate a well-conditioned system with minimal noise amplification. Since – for a given (angular) frequency $\omega$ and sonic speed $c$ – the sensor spacings are the only variables affecting the conditioning of matrix $\boldsymbol{A}$, the condition number $\kappa$ can serve as a design metric for sensor placement: by selecting appropriate sensor spacings, the measurement matrix can be made robust for the frequencies of interest, improving the reliability of reconstructed acoustic quantities.

Analytically, it can be shown that $\kappa$ is independent of the absolute distance $L_{3x}$ of the sensor array relative to the specimen – only the relative sensor spacings $L_{12}$ and $L_{23}$ affect numerical conditioning, as shown in Figure 3:

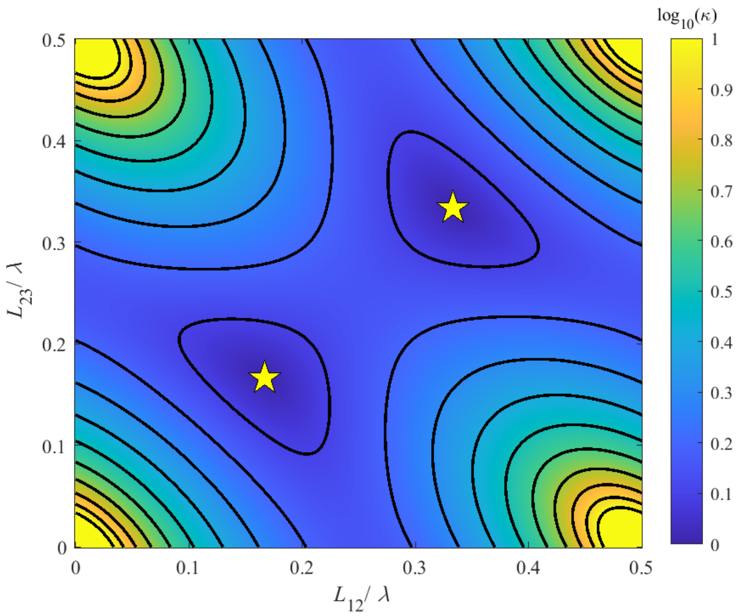


Figure 3: "Heatmap" of the condition number $\kappa$ for a TMM three-sensor array.

The theoretical minimum occurs when the three measured pressure phasors are spaced 120° apart. Under this condition, $\kappa = 1$, which corresponds to perfect numerical conditioning. To achieve this, the relative sensor spacings must be chosen to:

$$\frac{L_{12}}{\lambda} = \frac{L_{23}}{\lambda} = \frac{1}{6}. \tag{2.5}$$

In the equation above, $\lambda = c/f = 2\pi c/\omega$ refers to the wavelength. In practice, selecting sensor spacings close to $\lambda/6$ for a frequency of interest ensures low condition numbers and reliable results. Conversely, sensor spacings approaching 0 or multiple integers of $\lambda/2$ lead to near-linear dependence of the measurement rows and result in severe noise amplification. Physically, this occurs because the equation system "expects" practically identical pressures which – due to noise – will not be recorded in practice.

## 3. System-Level Model

Based on the fundamentals presented in section 2, a high-fidelity augmented 1D system model of the cooling circuit can be set up for system analysis and optimisation. Depending on the complexity of the respective component, either analytical or surrogate models from various sources are chosen to represent its passive properties in the system model, as it is shown in Figure 4:

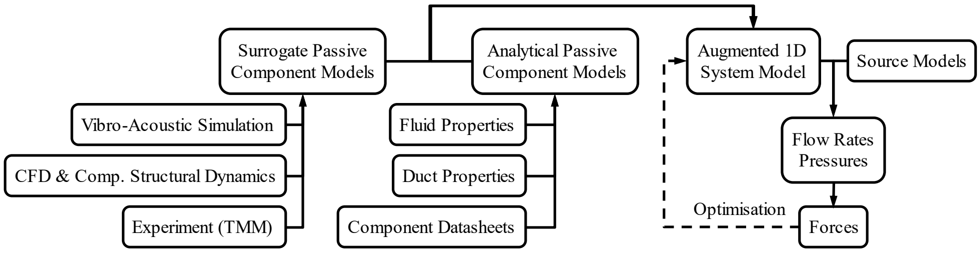


Figure 4: Data sources for the multidisciplinary augmented 1D system-level model.

## 3.1. Analytical Component Models

The geometry of most components of a duct system can be described by bulbous (i.e. acoustically "short", $fLc^{-1} \ll 1$) cuboids and slender cylinders. The acoustic behaviour of such components (e.g. tanks and pipes) can be estimated with sufficient confidence based on analytical relations alone. To parameterise the respective component models, the properties listed in Table 2 are required:

Table 2: Required properties for parameterisation of analytical component models.

| Category | Property |
|---|---|
| Fluid properties | Mass density $\rho$ |
| | Sonic speed $c$ or bulk modulus $K$ |
| | Viscosity $\eta$ or kinematic viscosity $\nu$ |
| Duct material properties | Young's modulus $E$ (potentially frequency-dependent and complex) |
| | Poisson's ratio $\mu$ |
| Duct geometry | Section length $L$ |
| | Inner diameter $d$ (or equivalent for non-circular sections) |
| | Wall thickness $e$ |
| Operational conditions | Average flow rate $\overline{Q}$ (to assess flow regime) |
| | Average fluid temperature $\overline{T}$ (for fluid properties) |
| | Mean pressure level $\overline{p}$ (for fluid properties) |

If the fluid is not a pure substance or a ubiquitously used, well-documented mixture, one must resort to e.g. manufacturer's data sheets to obtain the relationships between the thermodynamic state of the fluid and the respective fluid property.

## 3.2. Surrogate Component Models

In contrast to acoustically short or slender, tubular geometries, the transmission behaviour of components with complex internal geometries usually cannot be calculated purely by theory. In this case, surrogate component models have to be utilised. For the present system, the pump, the PVC hoses as well as the heat exchanger must be represented through surrogates.

### 3.2.1. Pump Surrogate Model

Like other positive displacement machinery, the pump's acoustic behaviour can be characterised through its source impedance (passive property) $Z_\mathrm{P}$ and its source flow ripple $Q_\mathrm{P}^*$ (active property, see section 3.3.1) according to a NORTON equivalent circuit [4]. Ideally, both these properties are determined experimentally through a TMM test setup as outlined in the standard ISO 10767-1:2015 [5]. If such measurements are not available (e.g. during the conceptual phase), reasonable estimates can often be made through semi-analytical approaches as shown below.

The source impedance $Z_\mathrm{P}$ of positive displacement pumps – as seen from the duct system – generally exhibits the characteristics of a simple hydraulic spring, damper and mass system:

$$Z_\mathrm{P} = \frac{C_\mathrm{P}}{\mathrm{i}\omega} + D_\mathrm{P} + \mathrm{i}\omega M_\mathrm{P} \tag{3.1}$$

The model parameters $C_\mathrm{P}$, $D_\mathrm{P}$ and $M_\mathrm{P}$ are directly related to the characteristics of the fluid enclosed between the gears and the pump flange. Due to the comparatively small size of the pump, the impedance will be governed by the hydraulic stiffness $C_\mathrm{P}$ in the frequency range of interest. This stiffness is typically substantially smaller than what would be expected from an estimate based on the enclosed fluid volume alone since the additional compliances of sealings and the pump casing are present. STULEMEIJER reports on the *effective fluid volume* of pumps with a known displacement volume per revolution [6]. This data can be used to construct a semi-empirical correlation to estimate the effective fluid volume of the pump in question and thus its hydraulic capacity. The dissipative and inertial contributions can be neglected here due to the pump's size and the frequencies of interest.

### 3.2.2. PVC Hose

The surrogate component model for the PVC hoses can be derived in three different ways: 1D theory (i.e. analytically), 3D vibro-acoustic analysis, or experimentally on the TMM test bench. The first two methods require knowledge of the geometry and the material behaviour of the hose, which is determined by a dynamic mechanical thermal analysis (DMTA). In contrast, the experiment on the TMM test bench does not require prior knowledge of the material behaviour of the hose or the geometry of the test specimen.

The results of the three different methods, represented as a mass-spring-mass model are shown in Figure 5. Differences between 1D theory and 3D vibro-acoustic simulation can be explained by the fact that 1D theory cannot capture 3D effects (e.g. ballooning at the transition from steel pipe to PVC hose). The experimental data from the TMM test bench is in good agreement with the other two methods. The stiffness $C$ from vibro-acoustic simulation aligns better with the measurement since the stiffness-enhancing clamping effect at both ends of the hose are taken into account. If at least another measurement with a different hose length is performed, a length-dependent surrogate model for the PVC hose can be derived.

The significant deviations between simulation and measurement at low frequencies can be explained by the increasingly bad condition number $\kappa$ (frequency range $f < 10$ Hz), while the low sensor coherence $\gamma^2$ – indicative of e.g. a low signal-to-noise ratio – explains the discrepancies at high frequencies (frequency range $f \geq 200$ Hz).

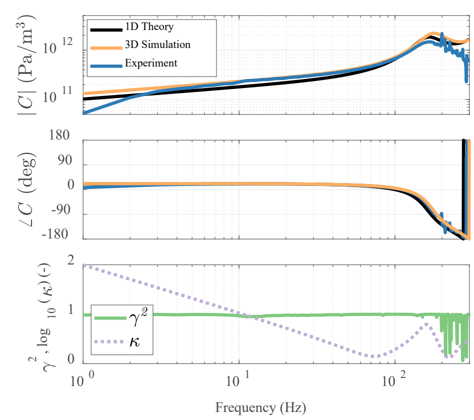


$$\boldsymbol{T}_{\text{Hose}} = \begin{bmatrix} 1 - \frac{M}{C}\omega^2 & M\mathrm{i}\omega\left(2 - \frac{M}{C}\omega^2\right) \\ \frac{\mathrm{i}\omega}{C} & 1 - \frac{M}{C}\omega^2 \end{bmatrix}$$

Figure 5: Comparison of various surrogate component models of the PVC hose.

### 3.2.3. Heat Exchanger Surrogate Model

As shown in Figure 6, the array of parallel narrow channels in the heat exchangers is connected via manifolds to the piping of the cooling circuit. Due to its highly branched and complex internal structure, a direct representation through a fully parametric TFM would be impractical and computationally inefficient. For this reason, the assembly of two heat exchangers and their respective manifolds is modelled through a surrogate model that extends from the “Inlet” to the “Outlet” port marked in Figure 6:

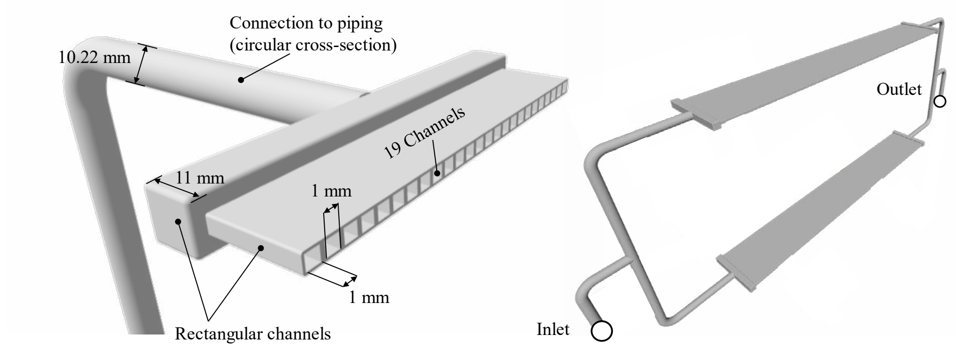


Figure 6: Heat exchanger cross-section with relevant dimensions.

The surrogate model is derived from a 3D vibro-acoustic simulation performed using commercially available FE software. Based on the calculated flow rates and pressures at the inlet and outlet of the heat exchanger assembly, the TFM elements of the surrogate model are determined using the same method as for experimental data (see section 2.4.1.).

## 3.3. Source Models

To obtain the pressures, flow rates and flow forces, the augmented 1D system model needs to be excited by source models. As outlined, several types of sources may excite liquid columns to oscillate. When modelling acoustic sources, a distinction is made between those of deterministic and those of stochastic nature. A typical example of a deterministic acoustic source is the flow ripple generated by the coolant pump.

### 3.3.1. Pump Flow Ripple

The coolant pump imposes a flow ripple phasor $Q_\mathrm{P}^*$ on the system boundary. For positive displacement pumps, the kinematic source flow ripple can often be reasonably approximated by a rectified sine wave with the amplitude $Q_\mathrm{P}'$ in the time domain. The sine amplitude is directly connected to the so-called degree of non-uniformity $\delta_\mathrm{P} = Q_\mathrm{P}'/\overline{Q}_\mathrm{P}$ commonly used in the pump industry [2]. The degree of non-uniformity $\delta_\mathrm{P}$ can be reasonably approximated based on the number of pumping elements $z$ (teeth per gear, pistons, etc.) by $\delta_\mathrm{P} = 2/z$ for $z \gg 1$. For the coolant pump at hand, $\delta_\mathrm{P} = 2/9 \approx 0.22$. Fourier decomposition of the assumed $Q_\mathrm{P}(t)$ shows that spectral contributions to the flow ripple amplitude spectrum (AS) only occur at integer multiples $n$ of the fundamental pumping frequency $f_\mathrm{P} = f_\mathrm{S} \cdot z$ (with $f_\mathrm{S}$ denoting the pump shaft frequency), and that their amplitudes decay with the square of the order $n$ as follows:

$$|Q_\mathrm{P}^*(n \cdot f_\mathrm{P})| = \frac{2}{\pi}\frac{\overline{Q}_\mathrm{P}\delta_\mathrm{P}}{4n^2 - 1} \tag{3.2}$$

### 3.3.2. Local Turbulence Sources

Even for nominally laminar flow throughout the system, strong deflections within a component may induce local turbulence (LT). These turbulent regions act as acoustic sources. In the investigated system, local turbulence occurs at the double bend and within the piping of the heat exchangers as depicted in Figure 1. The strength of local turbulence sources must be determined through CFD analysis or experimentally.

A common feature of sources due to local turbulence is their decay towards higher frequencies. Due to the randomness of the turbulent fluctuations, the corresponding sources show a stochastic behaviour, which is why they are characterised by a power spectral density (PSD) rather than an amplitude spectrum (AS). It is important to note that a PSD represents how the power of a signal is distributed across the frequency range. However, it *does not* represent a worst-case scenario that – for instance – can directly serve to calculate the maximum occurring pressure at a given location. Furthermore, it is not straightforward to combine deterministic and stochastic sources due to the different means of representation (amplitude and phase vs. PSD).

### 3.4. Pressures, Flow Rates & Forces

For the current model, one deterministic (pump) and two stochastic (local turbulence at the double bend and within the exchangers) sources are considered. Combining both deterministic and stochastic sources poses a particular challenge due to their different representations: Since a PSD does not contain any phase information anymore, a simple superposition of all sources is not guaranteed to provide the worst-case pressure and force amplitudes: Depending on the phase angle between the sources, superimposing them might result in constructive or destructive interference. To circumvent this issue, the relative phase angles of the stochastic sources with respect to the deterministic one are systematically varied which results in an envelope for the desired output quantities rather than single values.

This method is applied to the present system as well. The aim of the optimisation process is to minimise the axial reaction force amplitude $|F_{\mathrm{HE}}|$ at the heat exchangers which occurs primarily due to the pressure difference $\Delta p_{\mathrm{HE}} = p_{\mathrm{Inlet}} - p_{\mathrm{Outlet}}$ across them (see Figure 1 and Figure 6). Thus, the magnitude of the pressure difference $|\Delta p_{\mathrm{HE}}|$ at the heat exchanger is the hydraulic quantity of primary interest for the optimisation process. It is plotted as a function of the frequency in Figure 7. The dotted red curve shows the load case if only the pump source is active. The blue envelope band is obtained by adding the sources from local turbulence (heat exchangers and double bend) and varying their phase angles.

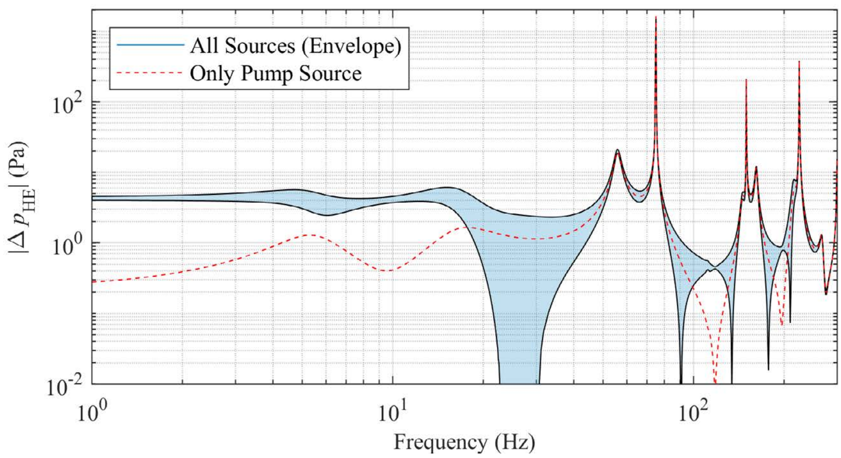


Figure 7: Baseline heat exchanger pressure difference $|\Delta p_{\mathrm{HE}}|$ as a function of the frequency.

As expected, the low-frequency range (below 20 Hz) is governed by the stochastic sources since these frequencies are well below the fundamental pumping frequency $f_{\mathrm{P}} = 75$ Hz. The distinct peaks due to pump excitation at 75 Hz and its harmonics (150 Hz, 225 Hz, …) are the most dominant contributions within the considered frequency range. When comparing the spectrum of the pressure difference (i.e. the forces on the laser source) with the characteristics of the control loop responsible for the laser beam orientation, the second-order peak at 150 Hz can be identified as the main driver of the precision loss of the prototype. Therefore, the goal of the following system optimisation will be the reduction of this peak.

## 4. Optimisation Workflow

Once the dominant force contributions and their causative sources are identified, targeted mitigation strategies can be derived. These measures are first evaluated virtually through surrogate-model enhanced 1D simulation. The innovative aspect of the proposed workflow is the ability to conduct rapid design iterations using a reduced-order system model while retaining the fidelity of full 3D simulations where necessary.

### 4.1. Hose Optimisation

A hose provides frequency-dependent compliance and damping through its viscoelastic material properties. Strategically positioning and sizing such a hose can attenuate pressure differences across sensitive components, thereby reducing the reaction force transmitted to the heat exchangers. This beneficial effect is to be maximised such that only minimal vibration affects the sensitive laser source. The optimisation problem possesses the following degrees of freedom:

- Hose length $L_{\mathrm{H}}$.
- Hose position $y_{\mathrm{H}}$, defined as the lateral distance of the bracket from the wall. The position affects local boundary conditions (e.g., support stiffness, damping) reflected in the section's transfer matrix.

The constraints are defined as follows:

- Box constraint on length of hose: 50 mm ≤ $L_{\mathrm{H}}$ ≤ 350 mm.
- Box constraint on position: 100 mm ≤ $y_{\mathrm{H}}$ ≤ 1900 mm.

The length of the viscoelastic hose is limited to prevent unwanted fluid-structure interaction. The limits for $y_{\mathrm{H}}$ are prescribed by layout rules and clearance envelopes (e.g., walls, frames, neighbouring equipment). In addition, the piping layout should be designed to route the flow directly to the heat exchanger, avoiding any detours or counterflow sections. Therefore, the axial constraint reads $L_{\mathrm{H}} + y_{\mathrm{H}} \leq 2100$ mm.

The optimisation problem of minimising the force magnitude at the heat exchangers is then given by $|F_{\mathrm{HE}}(f, L_{\mathrm{H}}, y_{\mathrm{H}})| \propto |\Delta p_{\mathrm{HE}}(f, L_{\mathrm{H}}, y_{\mathrm{H}})|$ and subject to the box constraints on $L_H$, $y_{\mathrm{H}}$, and the non-linear routing constraint. For the optimisation, a global *surrogate-based optimisation* with *adaptive sampling* is employed. Each evaluation of $|\Delta p_{\mathrm{HE}}(f, L_{\mathrm{H}}, y_{\mathrm{H}})|$ requires a frequency-domain simulation using the full transfer-matrix chain, which is computationally expensive and involves nonlinear constraint interactions (via position-dependent boundary conditions). The chosen approach proceeds as follows:

1. Evaluation of objective function: A set of quasi-random points is generated, and the objective function is evaluated at these points.
2. Interpolation for surrogate: A radial basis function (RBF) is used to interpolate the objective function to set up the surrogate model [7]. The cheap-to-evaluate surrogate approximates the expensive objective function.
3. After building the surrogate, the algorithm generates a large set of candidate points across the domain. Each candidate is scored using a merit function that balances

the predicted objective value from the surrogate and the distance from existing sample points. The candidate minimising the merit function is selected for true evaluation [8][9], and the surrogate is updated with this new data point.

The algorithm is repeated until a certain budget of evaluations is exhausted. This particular method is used since it is well suited for problems involving expensive evaluations, nonlinear constraints and unknown gradients.

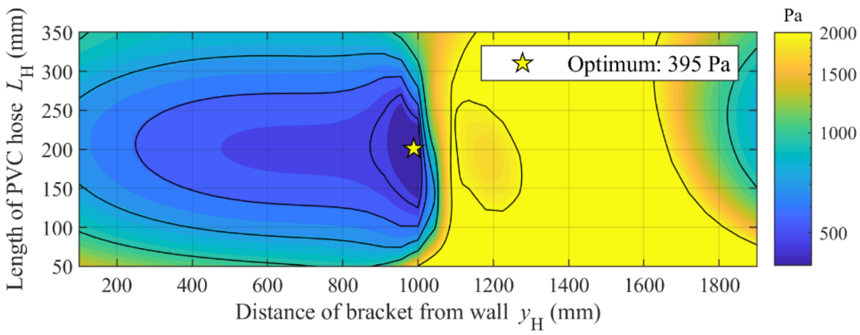


Figure 8: Contour plot of $|\Delta p_{\mathrm{HE}}|$ as a function of $y_{\mathrm{H}}$ and $L_{\mathrm{H}}$, optimum marked with star.

The optimisation results are depicted in Figure 8. The minimal pressure difference (and thus force) is obtained for a hose length $y_{\mathrm{H}} = 200$ mm and a wall distance of $L_{\mathrm{H}} = 1000$ mm for the bracket. With the optimisation, a setup with only 3.8 % of the maximum pressure difference – and thus force – on the heat exchangers (baseline pressure difference $|\Delta p_{\mathrm{HE}}| = 10400$ Pa) could be identified.

Intuitively, one would expect the hose-related pressure suppression to monotonically increase with the hose length and provide minimal forces when the suppression is directly *before* the evaluated points. However, since the hoses not only act as dissipative but also as reflective elements, the maximal suppression is reached at different location and length.

Following virtual testing, the most promising mitigation measure undergoes detailed mechanical design. A detailed 3D vibro-acoustic analysis of the final hose design is then carried out, enabling an assessment of the stress distribution and – in a subsequent analysis – fatigue life under realistic operating conditions which are obtained from the augmented 1D system model. This phase ensures mechanical integrity and durability, considering factors such as vibrational loads and dynamic stress concentrations.

## 4.2. Engineering Framework for Development, Validation and Industrialisation

In addition to the mitigation measures described above, the development of other suppression devices such as chamber-based or membrane-type silencers, might be necessary for other systems to address acoustic, vibrational, or flow-induced disturbances. In such cases, a systematic and multidisciplinary development process is recommended, encompassing mechanical design, material science, and the application of appropriate computer-aided engineering (CAE) methods, including coupled thermal, thermomechanical, and structural analyses, as well as reliability & lifetime assessment and industrialisation. Furthermore, the resulting components may need to be qualified and integrated for operation under non-standard environmental boundary conditions, including high- and low-temperature regimes, cleanroom environments, or vacuum conditions.

## 5. Conclusion & Outlook

In this paper, a comprehensive workflow for identifying and mitigating flow-related disturbances in cooling circuits for high-precision applications via multidisciplinary simulation was presented. By employing surrogate models, the high fidelity of 3D simulations and experimental investigations could be carried over to a multidisciplinary augmented 1D system model. By optimising the length and location of PVC hoses, a substantial reduction of performance-degrading force disturbances could be achieved. Future research may focus on further refining surrogate modelling techniques and exploring adaptive or actively actuated mitigation strategies to dynamically counteract varying operational conditions.

## 6. References

[1] Wylie, E. B., & Streeter, V. L. (1978). *Fluid transients*. New York.

[2] Theissen, H. (1984). *Die Berücksichtigung instationärer Rohrströmung bei der Simulation hydraulischer Anlagen.* (Doctoral dissertation, Rheinisch-Westfälische Technische Hochschule Aachen, Germany).

[3] Kojima, E., & Edge, K. A. (1994). Experimental determination of hydraulic silencer transfer matrices and assessment of the method for use as a standard test procedure. In *Innovations in Fluid Power: 7th Bath International Fluid Power Workshop.*

[4] Johnston, N., Dumnov, D., & Melling, J. (2023). Modelling of Pumps and Motors as Source Flow Ripple and Source Impedance. In *Fluid Power Systems Technology* (Vol. 87431, p. V001T01A008). American Society of Mechanical Engineers.

[5] International Organization for Standardization (2015). *Hydraulic fluid power — Determination of pressure ripple levels generated in systems and components — Part 1: Method for determining source flow ripple and source impedance of pumps*. (ISO Standard No. 10767-1:2015).

[6] Stulemeijer, I. P. J. M. (1981). *Beschreibung der Druckschwankungen in hydrostatischen Anlagen und ihre Auswirkungen auf den Luftschall*. (Doctoral dissertation, Technische Hogeschool Eindhoven, The Netherlands)

[7] Gutmann, H. M. (2001). A radial basis function method for global optimization. Journal of global optimization, 19(3), 201-227.

[8] Audet, C., & Dennis Jr, J. E. (2002). *Analysis of generalized pattern searches. SIAM Journal on optimization*, 13(3), 889-903.

[9] Abramson, M. A., Audet, C., Dennis Jr, J. E., & Digabel, S. L. (2009). *OrthoMADS: A deterministic MADS instance with orthogonal directions*. SIAM Journal on Optimization, 20(2), 948-966.

## Biographies

   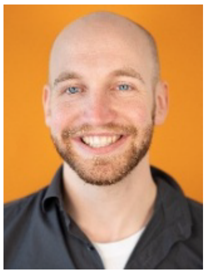

**Enrico Pasquini** received the bachelor's degree in mechanical engineering from FH Aachen University of Applied Sciences in 2010, the master's degree in aerospace engineering in 2014 and a PhD in mechanical engineering from RWTH Aachen University in 2020, respectively. He is currently working as a technical lead at the Department of Precision Engineering of AVL Deutschland GmbH. His research areas include duct acoustics and mathematical modelling.

**Jonas Wack** received the master's degree in mechanical engineering from Technical University of Munich in 2013 and a PhD in engineering from University of Stuttgart in 2020. He is currently working as a development engineer at the Department of Precision Engineering of AVL Deutschland GmbH. His research areas include duct acoustics and experimental methods.

**Afshin Sattarifar** received the bachelor's degree in mechanical engineering from University of Guilan/Iran in 2012, the master's degree in computational engineering in 2016 and a PhD in mechanical engineering in 2024 from Ruhr University Bochum. He is currently working as a development engineer at the Department of Precision Engineering of AVL Deutschland GmbH. His research areas include duct acoustics and structural health monitoring.

**Peter Gehr** received the master's degree in mechanical engineering from Regensburg University of Applied Sciences in 2020. He is currently working as a development engineer at AVL Software and Functions GmbH. His research areas include mathematical modelling and control engineering.